Ultralong α-MoO 3 Nanobelts: Synthesis and Effect of Binder Choice on Their Lithium Storage Properties

ARTICLE *in* THE JOURNAL OF PHYSICAL CHEMISTRY C · JUNE 2012

Impact Factor: 4.77 · DOI: 10.1021/jp304216z

3 AUTHORS, INCLUDING:

Zhiyu Wang
Dalian University of Technology
53 PUBLICATIONS **3,269** CITATIONS

SEE PROFILE

THE JOURNAL OF PHYSICAL CHEMISTRY C

Article

pubs.acs.org/JPCC

Ultralong α-MoO_3 Nanobelts: Synthesis and Effect of Binder Choice on Their Lithium Storage Properties

Zhiyu Wang,[†,‡] Srinivasan Madhavi,*[,‡] and Xiong Wen (David) Lou*[,†]

[†]School of Chemical and Biomedical Engineering, Nanyang Technological University, 70 Nanyang Drive, Singapore, 637457

[‡]School of Materials Science and Engineering, Nanyang Technological University, 50 Nanyang Avenue, Singapore, 639798

ABSTRACT: Ultralong α-MoO_3 nanobelts with an average length of 200−300 μm and uniform width of around 0.6−1.5 μm have been synthesized by a facile hydrothermal method using a molybdenum organic salt precursor. When evaluated for their lithium storage properties, the composite electrodes made from these nanobelts and bioderived polymer binders containing carboxy groups exhibit much better electrochemical performance than that composed of conventional poly(vinylidene fluoride) (PVDF) binder. Remarkably, the electrodes using sodium carboxymethyl cellulose (Na-CMC) binder can deliver the high specific capacity of over 730 mA h g^{-1} for over 200 cycles at a 0.2 C rate. Even cycled at high rates of 1−2 C, high capacities of around 430−650 mA h g^{-1} can be still retained. The positive effect of this type of binder on the electrode properties of α-MoO_3 nanobelts is further evidenced by using another bioderived binder, the sodium alginate (Na-alginate). Stable capacity retention of around 800 mA h g^{-1} for over 150 cycles at 0.2 C well-demonstrates that the choice of binder can greatly influence the electrochemical performance of metal oxide electrodes, especially those suffering from large volume expansion upon lithium intake.

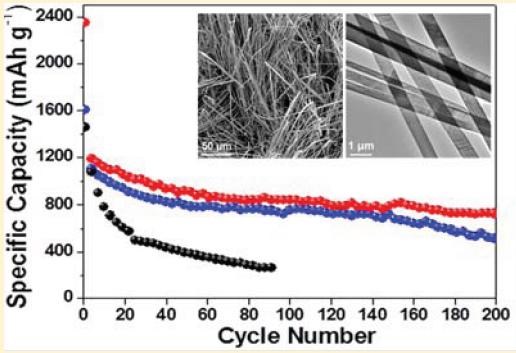

1. INTRODUCTION

Interstitial-free transitional metal oxides (TMOs) containing redox centers are promising anode materials in lithium-ion batteries (LIBs) due to their substantial advantages including high lithium storage capacity, widespread availability, and intrinsically enhanced safety by avoiding formation of hazardous lithium dendrite.[1−3] Depending on the lattice structure of metal oxides and thermodynamic and kinetic conditions, the mechanism for lithium storage in TMOs is mainly based on two types of reactions, namely, the addition-type insertion and the conversion reaction.[2−8] In the former case, Li^+ are reversibly inserted into the vacant sites of TMO frameworks without cleavage of M−O bonds. Although this process is highly kinetically favorable, it often suffers from a limited lithium storage capacity (generally below 200−300 mA h g^{-1}) due to the limited number of Li^+ that can be inserted. For the latter mechanism, metal oxides are completely reduced to metallic nanocrystals dispersed in a Li_2O matrix upon lithiation and then are reversibly restored to the oxidized state after delithiation. Benefiting from the fully utilized oxidation state and multiple electrons involved in the conversion reaction, the TMOs in this category manifest much higher specific capacities of 600−1200 mA h g^{-1} than that of carbonaceous materials (theoretical capacity, 372 mA h g^{-1}) and also a longer lifespan than the metal alloy electrodes. The major drawback of TMO anodes is the poor cycling stability for long-term and high-rate lithium storage, which is normally induced by the intrinsically poor electrical/ionic conductivity and drastic destruction of structure upon repeated lithium insertion/extraction. These disadvantages cause severe pulverization and polarization of the electrode. Thereby the electrode performance is deteriorated as a result of the loss of electrical conductivity and sluggish cycling response to high current rates. Although great efforts have been devoted to mitigate these problems by engineering TMO nanostructures with enhanced diffusion kinetics and structural stability, the development of truly durable TMO electrodes with satisfactory performance is still highly desirable.[3−6]

Molybdenum trioxide (MoO_3) is one of the most important TMOs due to its rich chemistry associated with multiple valence states and high thermal and chemical stability. It commonly exists in three polymorphs, namely, orthorhombic α-MoO_3, monoclinic β-MoO_3, and hexagonal MoO_3.[9] Previously, α-MoO_3 has long been used as the lithium storage host materials in view of the thermodynamically stable, intriguing layered structure. They are extensively employed as the cathode materials in LIBs to deliver the capacities of 200−300 mA h g^{-1} between 1.5 and 3.5 V on the basis of an intercalation mechanism.[10−18] Whereas anode materials α-MoO_3 have attracted much less attention because of the poor electrochemical properties caused by intrinsic sluggish kinetics for redox conversion reaction and large structure variation upon lithium insertion/extraction, despite that their theoretical capacity can be as high as 1117 mA h g^{-1}. Even for the electrodes composed of various nanostructures (e.g., the

Received: May 2, 2012
Revised: May 16, 2012
Published: May 22, 2012

   dx.doi.org/10.1021/jp304216z | J. Phys. Chem. C 2012, 116, 12508−12513

nanowires, micro-/nanorods, nanobelts, and nanoparticles),[19−26] severe capacity loss still happens at low current rates (often 0.02−0.2 C) despite the observed high initial capacity of 800−1000 mA h g^{-1}. Recently, fine MoO_3 nanoparticles (less than 20 nm in size) obtained by hot-wire chemical vapor deposition have been shown to exhibit excellent cycling stability at high rates of 0.5−2 C.[27] However, the production of truly durable α-MoO_3 electrodes with longer calendar life and improved high-rate performance still remains as a significant challenge at this moment.

Recent research suggests that the electrochemically inactive components such as ancillary binders also play a crucial role in determining the electrode performance. For example, the bioderived polymer binders containing carboxy groups, such as carboxymethyl cellulose (CMC) and alginate, have demonstrated promising characteristics to improve the electrochemical properties of Si or Fe_2O_3 based anodes regardless of their particle size.[28,29] The unique physiochemical properties and strong interaction of these binders with the active materials can effectively improve the structural stability and surface characteristics of the overall electrode, resulting in significantly enhanced electrode performance, although they are electrochemically inactive and their content in the electrode is quite low. For the electrodes based on TMOs, especially those suffering from huge structural variation upon lithium storage (e.g., α-MoO_3), the choice of an appropriate binder may be also critical for improving their electrochemical performance. However, only a limited number of works has focused on this aspect. In this work, we present the first synthesis of ultralong α-MoO_3 nanobelts by a hydrothermal method using a molybdenum organic salt (molybdenyl acetylacetonate) as the precursor. Interestingly, the obtained α-MoO_3 nanobelts have an ultralarge length of 200−300 μm, uniform width of 0.6−1.5 μm, but nanosized thickness. Previously, this has not been synthesized in solution with commonly used molybdenum inorganic salts (e.g., ammonium molybdate or sodium molybdate) as the precursor. The present study also shows that the choice of binder has great influence on the electrochemical performance of α-MoO_3 nanobelt based electrodes. The electrodes using sodium carboxymethyl cellulose (Na-CMC) and sodium alginate (Na-alginate) binders exhibit exceptional capacity retention of 700−800 mA h g^{-1} for 150−200 cycles, whereas, for the electrode made from a conventional binder (e.g., poly(vinylidene fluoride) (PVDF)), the capacity decays very fast to less than 400 mA h g^{-1} in a small number of cycles. Remarkably, the α-MoO_3 electrodes using Na-CMC binder can be cycled at a high rate of 1−2 C to deliver high capacities of 430−650 mA h g^{-1}, showing superior performance compared to other MoO_3 electrodes.[19−26]

2. EXPERIMENTAL SECTION

Materials Preparation. For the synthesis of ultralong α-MoO_3 nanobelts, 0.3 g of molybdenyl acetylacetonate was ultrasonically dispersed in a mixed solution of nitric acid (65 wt %, 15 mL) and deionized water (30 mL). The resulting suspension was transferred into a Teflon-lined stainless steel autoclave and heated at 200 °C for 20−25 h. After the reaction, the white product was harvested by several rinse−centrifugation cycles with deionized water and ethanol before drying at 60 °C.

Materials Characterization. The samples were characterized by field-emission scanning electron microscope (FESEM, JEOL, JSM-7600F), transmission electron microscope (TEM, JEOL, JEM-2010), and powder X-ray diffraction (XRD, Bruker, D8-Advance X-ray diffractometer, Cu Kα, λ = 1.5406 Å).

Electrochemical Measurements. The electrochemical measurements were conducted using two-electrode Swagelok cells with pure lithium foil as the counter and reference electrodes at room temperature. The working electrode consists of the α-MoO_3 nanobelts, carbon black (Super-P-Li), and the binder in a weight ratio of 7:2:1. Three binders, including Na-CMC, Na-alginate, and PVDF, were used for the comparative study. The electrolyte used is 1.0 M $LiPF_6$ in a 50:50 (w/w) mixture of ethylene carbonate and diethyl carbonate. The galvanostatic charge/discharge tests were performed using a Neware battery tester at different current rates with a cutoff voltage window of 0.01−3.0 V.

3. RESULTS AND DISCUSSION

The crystallographic structure and phase purity of MoO_3 samples are determined by X-ray powder diffraction (XRD), as shown in Figure 1. All of the diffraction peaks can be

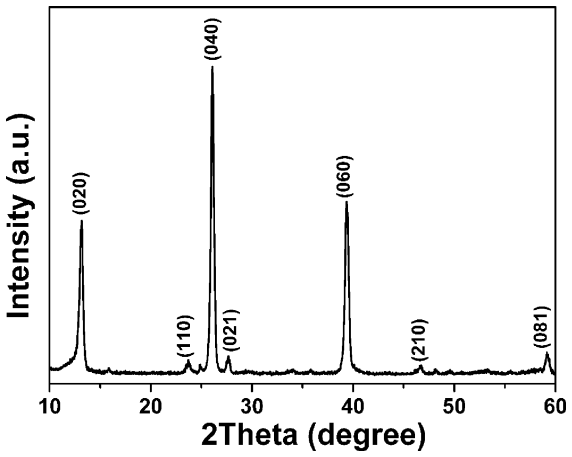

Figure 1. XRD pattern of ultralong α-MoO_3 nanobelts.

perfectly assigned to orthorhombic α-MoO_3 (JCPDS card no. 05-0508). The absence of noticeable impurity peaks suggests the high purity of the α-MoO_3 product. The stronger intensities of the (020), (040), and (060) diffraction peaks suggest the highly anisotropic growth of the nanostructures.[9] The morphology and structure of the α-MoO_3 samples are characterized with field-emission scanning electron microscopy (FESEM), as shown in Figure 2a−c. A panoramic view reveals that the sample consists entirely of uniform nanobelts without impurity particles or aggregates. These structures are confirmed to be nanobelts since their projected width changes accompanying the rotation around the axes, implying a rectangular cross-section instead of a round one (Figure 2d). Interestingly, these nanobelts have an average length of as long as 200−300 μm with uniform width of 0.6−1.5 μm, corresponding to a high aspect ratio of around 200−500. The TEM images further evidence the beltlike shape of the as-obtained α-MoO_3 nanostructures (Figure 3a,b). Precise determination of the belt thickness is difficult here since nearly all of the belts are lying flat on the support due to their small thickness. Approximately, it is estimated to be 20−40 nm on the basis of the FESEM image of curved belts (Figure 2d). The selected-area electron diffraction (SAED) analysis on a single nanobelt gives a pattern appearing as a regular array of diffraction spots along the ⟨010⟩ zone axis of the α-MoO_3

dx.doi.org/10.1021/jp304216z | J. Phys. Chem. C 2012, 116, 12508−12513

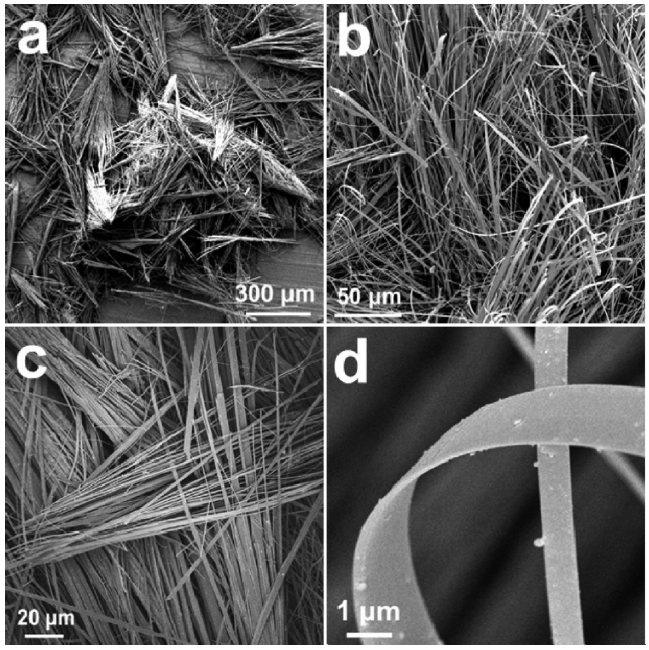

Figure 2. (a–c) FESEM images of ultralong α-MoO_3 nanobelts synthesized at 200 °C for 25 h; (d) a freestanding nanobelt with small thickness.

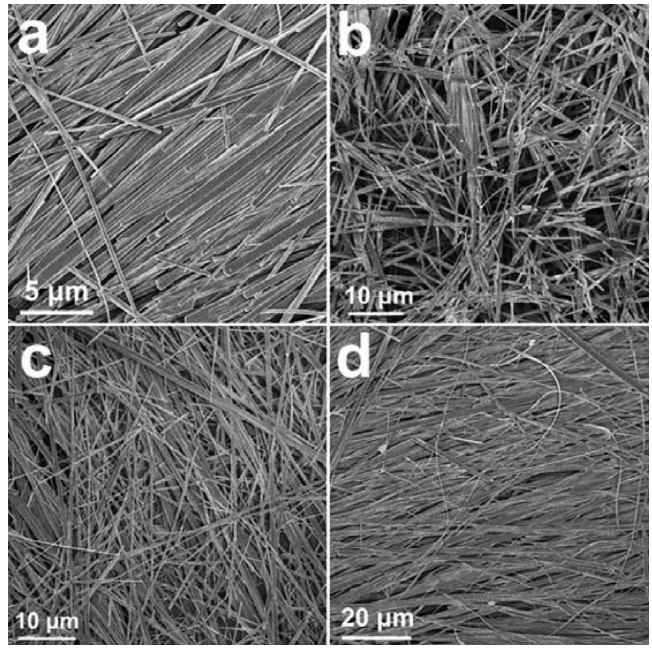

Figure 4. FESEM images of the α-MoO_3 samples prepared at 200 °C after reaction for different durations: (a) 5, (b) 10, (c) 15, and (d) 20 h.

crystal (Figure 3c), indicating the highly single-crystalline nature. From this analysis, it can also be determined that the long axis of the nanobelts is along the [001] direction. The favorable growth of α-MoO_3 along the [001] direction is determined by its highly anisotropic crystal structure.[9] In α-MoO_3, distorted [MoO_6] octahedra share four corners to form a plane and two planes join together by sharing octahedral edges along the [001] direction. All of these bilayers stack up along the [010] direction with weak van der Waals forces.[9,30] From the energy point of view, the planar growth rates along axes of the α-MoO_3 crystal have the following sequence {001} > {100} > {010}; therefore, it is highly favorable for α-MoO_3 crystal to grow along the [001] direction forming beltlike structures with the largest exposed surface of {010} facets.[9,31]

The major factors involved in the growth of ultralong α-MoO_3 nanobelts are the reaction time and temperature. FESEM examination shows that, after the reaction for 5–10 h, only α-MoO_3 nanorods with a length of 30–40 μm are formed in solution due to the insufficient growth, as shown in Figure 4a,b. Prolonging the reaction to 15–20 h, much longer α-MoO_3 nanobelts (100–200 μm in length) appear as a result of dominant crystal growth along the [001] direction (Figure 4c,d). Considering α-MoO_3 is constructed by stacking bilayers of [MoO_6] octahedra via van der Waals interaction, their {010} surfaces may possess a strong tendency for external bonding with the organic species released from the decomposition of molybdenum organic salt. This may also inhibit the growth of α-MoO_3 crystals along the [010] direction. Thus, ultralong nanobelts instead of nanowires are eventually formed after reaction for 25 h. In this process, a high temperature is necessary for sufficient decomposition of the molybdenum organic salt because their decomposition temperature is higher than that of inorganic precursors.[32] A lower temperature, e.g., 180 °C, causes slow and insufficient decomposition of molybdenum organic salts, leading to the formation of short α-MoO_3 nanorods (Figure 5a), while, at a higher temperature of 220 °C, the nanobelts with much larger width (over 10 μm) are obtained due to the excessive growth of α-MoO_3 crystal along the [100] direction in solution (Figure 5b). Moreover, the organic molybdenum precursor itself also plays a critical role for the formation of ultralong MoO_3 nanobelts. With inorganic molybdenum precursor (e. g., ammonium molybdate), only nanorods with a length of tens of micrometers can be synthesized under identical conditions, as shown in Figure

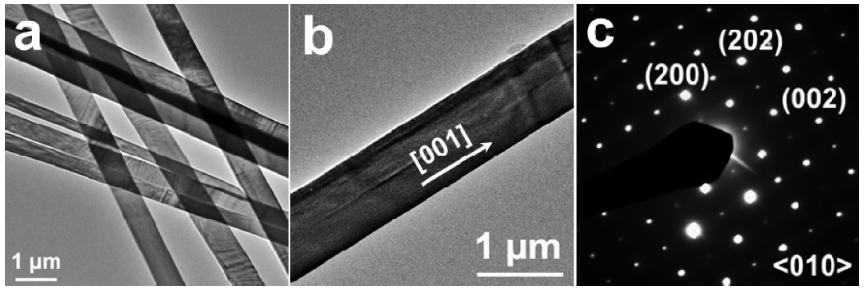

Figure 3. (a) TEM image of ultralong α-MoO_3 nanobelts; (b) top view of a nanobelt grown along the [001] direction; (c) the corresponding SAED pattern along the ⟨010⟩ zone axis.

dx.doi.org/10.1021/jp304216z | J. Phys. Chem. C 2012, 116, 12508–12513

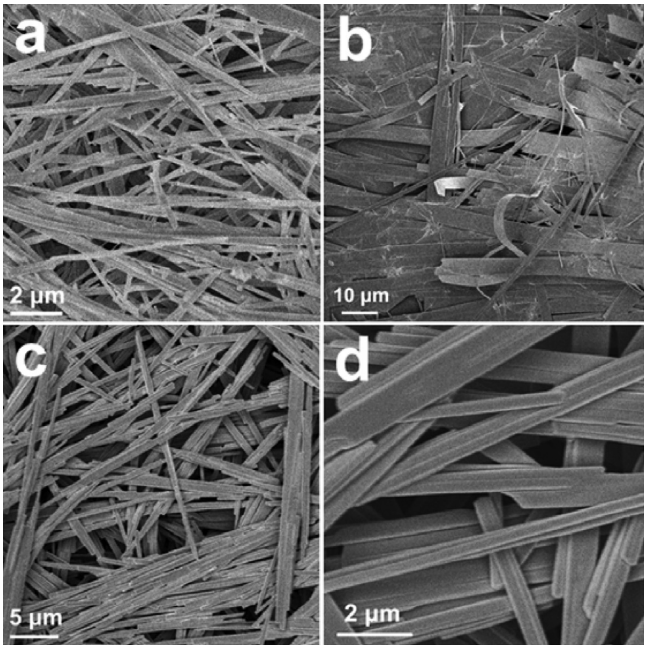

Figure 5. FESEM images of the α-MoO_3 samples prepared at (a) 180 and (b) 220 °C for 25 h. The α-MoO_3 products synthesized from ammonium molybdate at 200 °C for 25 h are shown in c and d.

5c,d. We speculate that the adsorption of organic species released from the decomposition of molybdenyl acetylacetonate can stabilize the surface of MoO_3 crystals, which favors the growth of very long nanobelts by protecting them from dissolution in the acidic solution.

In view of the great promise of α-MoO_3 in lithium storage, the electrochemical lithium storage properties of these nanobelts are also investigated. Their first and second discharge/charge voltage profiles are shown in Figure 6a. The initial discharge and charge capacities are found to be 2349 and 1126 mA h g^{-1}, respectively, at a 0.2 C rate within a cutoff voltage window of 0.01−3.0 V. The large capacity loss in the first cycle is mainly attributed to the irreversible intercalation of Li^+ ions into the crystal lattice and the formation of Li_2O, as well as other irreversible processes such as inevitable formation of solid−electrolyte interface (SEI) layer and electrolyte decomposition, which are common for most TMO anodes[19−26] and can be readily mitigated by prelithiation of the electrode for practical use.[33] The discharge curve for the first cycle can be divided into two regions. In the region above 1.5 V (region I), approximately 1.2 Li is inserted into the α-MoO_3 with two discrete small plateaus at around 2.6 and 2.2 V, corresponding to the intercalation of Li^+ into the interlayer spacing between $[MoO_6]$ bilayers and crystal lattice (probably into the $[MoO_6]$ bilayers).[11,18] As the potential decreases to below 1.5 V (region II), redox conversion reaction takes place to exhibit a long plateau at around 0.4−0.5 V. Once the conversion reaction ends, the structure of active materials transform completely into amorphous, resulting in smooth voltage profiles for the first charge process and subsequent cycles. To further understand the electrochemical route for lithium storage in α-MoO_3 nanobelts, the differential capacity versus voltage curves for the first and second cycles are plotted in Figure 6b. Two peaks at around 2.6 and 2.2 V are visible in the first cycle but indiscernible in the subsequent cycles, indicating the addition-type reaction in region I is irreversible partly because the crystalline structure is completely destroyed during the discharge below 1.5 V. The pronounced peaks at around 0.4 V is assigned to the redox conversion reaction, and it shifts negatively to around 0.3 V after the first cycle. This

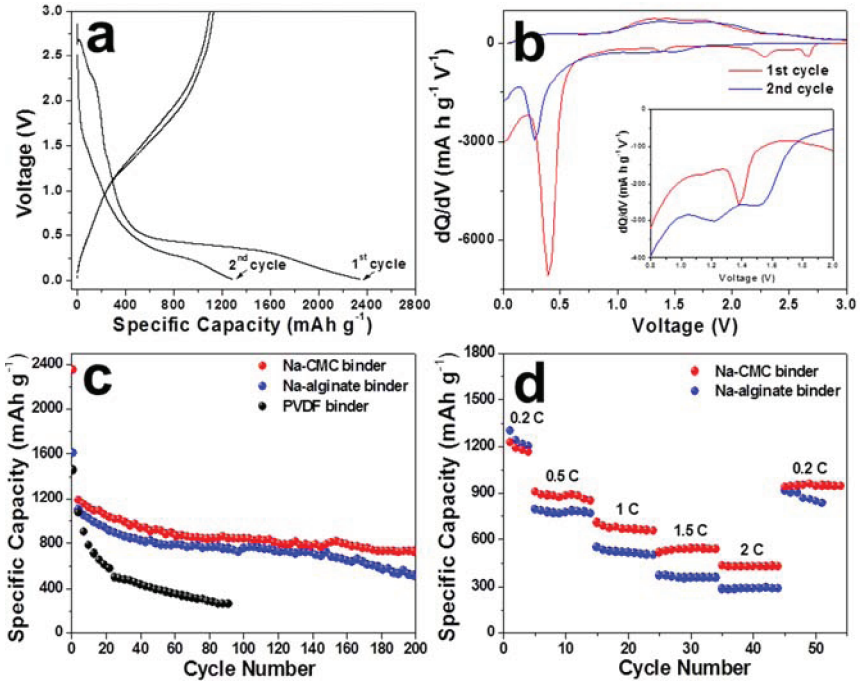

Figure 6. (a) Discharge/charge voltage profiles of ultralong α-MoO_3 nanobelts using Na-CMC as the binder; (b) the corresponding differential capacity versus voltage curve, of which the inset is the enlarged view between 0.8 and 2.0 V; (c) cycling performance of these nanobelts with different binders, Na-CMC, Na-alginate, and PVDF (all these tests were conducted at a 0.2 C rate within a cutoff voltage window of 0.01−3.0 V; (d) rate capability of ultralong MoO_3 nanobelts with two binders, Na-CMC and Na-alginate, which are tested within 0.01−3.0 V.

dx.doi.org/10.1021/jp304216z | J. Phys. Chem. C 2012, 116, 12508−12513

phenomenon is unusual for TMOs because of the more favorable kinetics for Li^+ and O^{2-} diffusion in amorphous structure normally leading to increased lithiation equilibrium potential.[20,34] We explain this observation by the change of chemical composition of α-MoO_3 during the conversion reaction. To clarify this, the enlarged view of the differential capacity versus voltage curves in the range of 0.8−2.0 V is plotted in the inset of Figure 6b. The weak peaks at around 1.2−1.5 V strongly suggest the formation of a MoO_2 phase because this reaction potential corresponds to the electrochemical reaction of MoO_2.[35−37] Compared to α-MoO_3, MoO_2 is less reactive for lithiation due to the lower equilibrium potential (1.6 V for MoO_2 and 1.83 V for MoO_3) but higher activation barrier.[20] Its presence reasonably reduces the electrochemical reactivity of molybdenum oxides, leading to the decrease in the conversion reaction potential and rapid capacity decay of the nanobelt electrodes in the initial cycles. Overall, the electrochemical route for the lithium storage reaction in α-MoO_3 nanobelts can be described as follows:[25]

$$MoO_3 + xLi^+ + xe^- \rightarrow Li_xMoO_3 \quad (1)$$

$$Li_xMoO_3 + (6-x)Li^+ + (6-x)e^- \leftrightarrow Mo + 3Li_2O \quad (2)$$

The α-MoO_3 electrode using the Na-CMC binder shows excellent cycling performance between 0.01 and 3 V at a 0.2 C rate, as characterized by the high capacity of over 730 mA h g^{-1} for over 200 cycles (Figure 6c). Even cycled at high rates of 1−2 C, the capacities of 430−650 mA h g^{-1} can still be retained (Figure 6d). This value is much higher than the theoretical capacity of graphite (372 mA h g^{-1}) and superior to most of the molybdenum oxide anodes reported.[19−26] The positive effect of bioderived binders on the electrode properties of α-MoO_3 nanobelts is further evidenced by using the Na-alginate binder. Stable capacity retention of around 800 mA h g^{-1} for over 150 cycles at 0.2 C can be achieved in this case, whereas, for the electrode using normal PVDF binder, the capacity fades rapidly to less than 400 mA h g^{-1} within only 20 cycles under identical test conditions. The significant difference among the electrodes made with different binders indicates that the choice of binder is critical to determine the electrochemical performance of α-MoO_3, and perhaps other TMOs. Although the PVDF works well for commercialized carbonaceous materials with small volume change (<10%), it is perhaps not the best for metal oxide electrodes with huge volume variation during charging/discharging. As the binders for electrode construction, Na-CMC and Na-alginate exhibit intrinsic advantages over the conventional PVDF binder. For example, these polymers can dissolve in water with a fully stretched molecular conformation because of the rigid long chains and the electrostatic repulsive interactions between ionized carboxy groups.[28,38] This unique structural feature facilitates the formation of homogeneous three-dimensional networking between the conductive agent and active material particles, resulting in a tightened electrode architecture.[38] In contrast, the electrode with PVDF binder suffers from heterogeneous material dispersion and poor mechanical strength as a result of insufficient bridging of the electrode materials with flexible, coil-shape chains. Moreover, these carbohydrate-based polymers have a strong tendency to bond with active material particles and the current collector due to the presence of abundant polar functional groups.[39,40] Such interactions may contribute to the stable lithium storage capability by protecting the networking structure within the electrode from dislocation, minimizing the volume changes of active material particles and self-healing the local electrode destruction.[28,39,40] For MoO_3 nanobelts, the hydrogen bonding between oxygen-terminated {010} facets and carboxyl group (generated from the hydrolysis of the -COONa group) of CMC or alginate molecules might be important. In addition, the interaction between these binders and the electrolyte may also improve the electrode performance by assisting in building a deformable and stable SEI layer on the surface of active materials and decreasing the interfacial resistance as a polyelectrolyte.[28,41,42] The synergy and interplay of these effects greatly improve the structural stability and surface characteristics of TMO electrodes; thus, exceptional long-term cycling stability and improved high-rate performance are anticipated.

4. CONCLUSIONS

In summary, ultralong α-MoO_3 nanobelts have been synthesized by a simple hydrothermal method using a molybdenum organic salt as the precursor. These nanobelts are single-crystalline grown along the [001] direction. The nanobelts can be as long as 200−300 μm, and the width is as uniform as 0.6−1.5 μm. The composite electrodes made from these α-MoO_3 nanobelts and bioderived binders such as Na-CMC and Na-alginate exhibit very stable capacity retention of over 700−800 mA h g^{-1} for over 200 cycles, whereas the electrode made from the conventional PVDF binder suffers from rapid capacity decay in a small number of cycles under identical test conditions. Remarkably, the α-MoO_3 electrode using the Na-CMC binder can be cycled at high current rates of 1−2 C to deliver high capacities of 430−650 mA h g^{-1}. It is clear that the choice of polymer binder is very critical in optimizing the performance of metal oxide electrodes, especially for those undergoing drastic volume and structure changes upon lithiation. The comprehensive evaluation of high-capacity metal oxide electrodes using different binder systems is thus highly meaningful and desirable for the development of high-performance lithium-ion batteries.

AUTHOR INFORMATION

Corresponding Author

*E-mail: madhavi@ntu.edu.sg (S.M.); xwlou@ntu.edu.sg (X.W.L.).

Notes

The authors declare no competing financial interest.

ACKNOWLEDGMENTS

The authors are grateful to the National Research Foundation (Singapore) for financial support through the Clean Energy Research Programme (CERP; Grant NRF2009EWTCERP001-036).

REFERENCES

(1) Poizot, P.; Laruelle, S.; Grugeon, S.; Dupont, L.; Tarascon, J. M. *Nature* **2000**, *407*, 496.
(2) Ku, J. H.; Jung, Y. S.; Lee, K. T.; Kim, C. H.; Oh, S. M. *J. Electrochem. Soc.* **2009**, *156*, A688.
(3) Wang, Z. Y.; Zhou, L.; Lou, X. W. *Adv. Mater.* **2012**, *24*, 1903.
(4) Cheng, F. Y.; Liang, J.; Tao, Z. L.; Chen, J. *Adv. Mater.* **2011**, *23*, 1695.
(5) Bruce, P. G.; Scrosati, B.; Tarascon, J. M. *Angew. Chem., Int. Ed.* **2008**, *47*, 2930.
(6) Guo, Y. G.; Hu, J. S.; Wan, L. J. *Adv. Mater.* **2008**, *20*, 2878.

(7) Liu, H.; Wang, G. X.; Liu, J.; Qiao, S. Z.; Ahn, H. *J. Mater. Chem.* **2011**, *21*, 3046.
(8) Liu, H.; Du, X. W.; Xing, X. R.; Wang, G. X.; Qiao, S. Z. *Chem. Commun. (Cambridge, U. K.)* **2012**, *48*, 865.
(9) Lou, X. W.; Zeng, H. C. *Chem. Mater.* **2002**, *14*, 4781.
(10) Tsumura, T.; Inagaki, M. *Solid State Ionics* **1997**, *104*, 183.
(11) Li, W. Y.; Cheng, F. Y.; Tao, Z. L.; Chen, J. *J. Phys. Chem. B* **2006**, *110*, 119.
(12) Kerr, T. A.; Wu, H.; Nazar, L. F. *Chem. Mater.* **1996**, *8*, 2005.
(13) Reddy, C. V. S.; Walker, E. H., Jr.; Wen, C.; Mho, S. *J. Power Sources* **2008**, *183*, 330.
(14) Mai, L. Q.; Hu, B.; Chen, W.; Qi, Y. Y.; Lao, C. S.; Yang, R. S.; Dai, Y.; Wang, Z. L. *Adv. Mater.* **2007**, *19*, 3712.
(15) Chen, J. S.; Cheah, Y. L.; Madhavi, S.; Lou, X. W. *J. Phys. Chem. C* **2010**, *114*, 8675.
(16) West, W. C.; Whitacre, J. F. *J. Electrochem. Soc.* **2005**, *152*, A966.
(17) Dewangan, K.; Sinha, N. N.; Sharma, P. K.; Pandey, A. C.; Munichandraiah, N.; Gajbhiye, N. S. *CrystEngComm* **2011**, *13*, 927.
(18) Zhou, L.; Yang, L. C.; Yuan, P.; Zou, J.; Wu, Y. P.; Yu, C. Z. *J. Phys. Chem. C* **2010**, *114*, 21868.
(19) Mai, L. Q.; Yang, F.; Zhao, Y. L.; Xu, X.; Xu, L.; Hu, B.; Luo, Y. Z.; Liu, H. Y. *Mater. Today* **2011**, *14*, 346.
(20) Jung, Y. S.; Lee, S.; Ahn, D.; Dillon, A. C.; Lee, S. *J. Power Sources* **2009**, *188*, 286.
(21) Tao, T.; Glushenkov, A. M.; Zhang, C. F.; Zhang, H. Z.; Zhou, D.; Guo, Z. P.; Liu, H. K.; Chen, Q. Y.; Hu, H. P.; Chen, Y. *J. Mater. Chem.* **2011**, *21*, 9350.
(22) Hassana, M. F.; Guo, Z. P.; Chen, Z.; Liu, H. K. *J. Power Sources* **2010**, *195*, 2372.
(23) Fang, L.; Shu, Y. Y.; Wang, A. Q.; Zhang, T. *J. Phys. Chem. C* **2007**, *111*, 2401.
(24) Xue, X. Y.; Chen, Z. H.; Xing, L. L.; Yuan, S.; Chen, Y. J. *Chem. Commun. (Cambridge, U. K.)* **2011**, *47*, 5205.
(25) Riley, L. A.; Lee, S. H.; Gedvilias, L.; Dillon, A. C. *J. Power Sources* **2010**, *195*, 588.
(26) Li, X. L.; Liu, J. F.; Li, Y. D. *Appl. Phys. Lett.* **2002**, *81*, 4832.
(27) Lee, S. H.; Kim, Y. H.; Deshpande, R.; Parilla, P. A.; Whitney, E.; Gillaspie, D. T.; Jones, K. M.; Mahan, A. H.; Zhang, S. B.; Dillon, A. C. *Adv. Mater.* **2008**, *20*, 3627.
(28) Kovalenko, I.; Zdyrko, B.; Magasinski, A.; Hertzberg, B.; Milicev, Z.; Burtovyy, R.; Luzinov, I.; Yushin1, G. *Science* **2011**, *334*, 75.
(29) Li, J.; Dahn, H. M.; Krause, L. J.; Le, D.; Dahn, J. R. *J. Electrochem. Soc.* **2008**, *155*, A812.
(30) Hu, S.; Ling, X.; Lan, T.; Wang, X. *Chem.—Eur. J.* **2010**, *16*, 1889.
(31) Cheng, L.; Shao, M. W.; Wang, X. H.; Hu, H. B. *Chem.—Eur. J.* **2009**, *15*, 2310.
(32) Park, J. C.; Song, H. *Chem. Mater.* **2007**, *19*, 2706.
(33) Hassoun, J.; Lee, K.; Sun, Y.; Scrosati, B. *J. Am. Chem. Soc.* **2011**, *133*, 3139.
(34) Wang, Z. Y.; Luan, D. Y.; Madhavi, S.; Hu, Y.; Lou, X. W. *Energy Environ. Sci.* **2012**, *5*, 5252.
(35) Wang, Z. Y.; Chen, J. S.; Zhu, T.; Madhavi, S.; Lou, X. W. *Chem. Commun. (Cambridge, U. K.)* **2010**, *46*, 6906.
(36) Auborn, J. J.; Barberio, Y. L. *J. Electrochem. Soc.* **1987**, *134*, 638.
(37) Dahn, J. R.; McKinnon, W. R. *Solid State Ionics* **1987**, *23*, 1.
(38) Lestriez, B.; Bahri, S.; Sandu, I.; Roué, L.; Guyomard, D. *Electrochem. Commun.* **2007**, *9*, 2801.
(39) Hochgatterer, N. S.; Schweiger, M. R.; Koller, S.; Raimann, P. R.; Wöhrle, T.; Wurm, C.; Winter, M. *Electrochem. Solid-State Lett.* **2008**, *11*, A76.
(40) Bridel, J. S.; Azaïs, T.; Morcrette, M.; Tarascon, J. M.; Larcher, D. *Chem. Mater.* **2010**, *22*, 1229.
(41) Li, J.; Lewis, R. B.; Dahn, J. R. *Electrochem. Solid-State Lett.* **2007**, *10*, A17.
(42) Chou, S. L.; Wang, J. Z.; Liu, H. K.; Dou, S. X. *J. Phys. Chem. C* **2011**, *115*, 16220.